Geomechanics and Engineering, *Vol. 31, No. 1 (2022) 71-86*
https://doi.org/10.12989/gae.2022.31.1.071

Investigation of slope reinforcement with drilled shafts in colluvium soils

An-Jui Li[a], Wei-Chien Wang* and Horn-Da Lin[b]

Department of Civil and Construction Engineering, National Taiwan University of Science and Technology, No.43, Keelung Rd., Sec.4, Da'an Dist., Taipei City, Taiwan R.O.C.

(*Received May 3, 2021, Revised July 12, 2022, Accepted September 18, 2022*)

Abstract. In Taiwan, an efficient approach for enhancing the stability of colluvium slopes is the drilled shaft method. For slopes with drilled shafts, the soil arching effect is one of the primary factors influencing slope stability and intertwines to the failure mechanism of the pile-soil system. In this study, the contribution of soil arching effect to slope stability is evaluated using the FEM software (Plaxis 3D) with the built-in strength reduction technique. The result indicates the depth of the failure surface is influenced by the S/D ratio (the distance to the diameter of piles), which can reflect the contribution of the soil arching effect to soil stability. When α (rock inclination angles)=β (slope angles) is considered and the S/D ratio=4, the failure surface of the slope is not significantly influenced by the piles. Overall, the soil arching effect is more significant on α=β, especially for the steep slopes. Additionally, the soil arching effect has been included in the proposed stability charts. The proposed charts were validated through two case studies, including that of the well-known Woo-Wan-Chai field in Taiwan. The differences in safety factor (FoS) values between the referenced literature and this study was approximately 4.9%.

Keywords: colluvium; drilled shaft; failure mechanism; soil arching effect; stability charts

1. Introduction

Cho (2016) emphasized that geotechnical engineering plays an important role in sustainable development to reduce climate change and energy depletion. One of the representative examples is disaster prevention and mitigation, such as floods and landslides due to earthquakes, tsunamis, typhoons, and heavy rainfall. Because of the unique geographical environment and relatively young geology of Taiwan, weathered rocks roll and accumulate to form colluvial soil. In general, colluvium is loose and highly permeable, incidences of colluvium slope failure occur when Taiwan is hit by typhoons. Data from the Soil and Water Conservation Bureau, Council of Agriculture, Executive Yuan, reveal that 198 incidences of colluvium slope failure, which resulted in 873 casualties, occurred due to typhoons or heavy rainfall in Taiwan between 2008 and 2017 (https://www.swcb.gov.tw/Statistics/item_list?mid=220). Compared to other slope stabilization methods (e.g., retaining walls, anchors, etc.), using drilled shafts to stabilize slopes is more sustainable and eco-friendly due to less excavation, low vibration, low noise, and low maintenance. In addition, it is an effective remedy to improve slope stability especially when the sliding surface for the unreinforced slope is relatively shallow (Ausilio *et al.* 2001) such as colluvium slopes in Taiwan. Therefore, it is a popular method to stabilize slopes in Taiwan.

Stabilizing piles, also referred as passive piles, are loaded by lateral movement of surrounding soil. These piles transfer body and shear forces from the soil mass to underlying stable layers maintaining the stability of the soil mass to underlying stable layers, maintaining the stability of the landslide. Relevant studies on stabilization piles mainly include soil-pile interaction, contribution to slope stability, and soil arching effect. Generally, the analysis methods of stabilizing piles are categorized into four groups (Steward 1992).

• Empirical method: The method needs empirical design chart and the design chart cannot be used if the specific site condition is different from the site condition from which the data was obtained. Furthermore, the empirical method cannot take into account of the effects such as the pile spacing, pile dimensions, and slope angle. (Nakamura 1984, Stewart *et al.*1994)

• Earth pressure-based method: The method involves the stability analysis of both the slope and pile. The major problem involved is the determination of lateral load acting on a pile. The current design practices for the design of slopes stabilized with a single row of piles often use the limit equilibrium method, where the soil-pile interaction is not considered, and the piles are assumed to only supply additional sliding resistance (Ito *et al.* 1975, Steward *et al.* 1994, Poulos 1995, Lee *et al.* 1995, Chow 1996, Hassiotis *et al.* 1997, Ausilio *et al.* 2001, Ashour and Ardalan 2012). Based on the studies of Hassiotis *et al.* (1997), Ausilio *et al.* (2001), limit equilibrium method and limit analysis method are used to evaluate the contribution of piles on slope stability, respectively. In their approaches, the 2D model is used and the stabilizing force of piles was pre-assumed. Therefore, the soil arching effect and the failure mechanism of pile-soil system are not available to consider in these

*Corresponding author, Ph.D. Candidate
E-mail: d10305001@mail.ntust.edu.tw
[a]Associate Professor
[b]Professor

ISSN: 2005-307X (Print), 2092-6219 (Online)

methods. On the other hand, Ashour and Ardalan (2012) proposed a new procedure for the analysis of slope stabilization using piles. The developed method allows to account for the influence of pile spacing on the interaction between the pile and surrounding soils and pile capacity, but the failure mechanism of pile-soil system is still not available to be considered.

• Displacement-based method: The method is a half empirical method and accurate description of free field soil movements is a priori which is extremely difficult to do. (Stewart *et al.* 1994, Lee *et al.* 1995, Chow 1996)

• Finite element method (FEM): Compared to mentioned three methods, the method is a better approach to analyze the interactive system of soil and pile. (Chen and Martin 2002, Liang and Zeng 2002, Liang and Yamin 2010) In fact, the soil arching effect is a three-dimensional (3D) effect between soils and piles, so using FEM is a direct method without artificial assumptions (e.g., pre-assumed failure mechanism or shape of earth pressure, etc.) to evaluate the soil arching effect and to investigate the failure mechanism of pile-soil system. Recently, some studies (Gholampour and Johari 2019, Johari *et al.* 2020, Johari and Kalantari 2021) adopt random FEM to discuss the soil-structure (such as soil nail and soldier pile) system reliability. Using stochastic analysis to examine the effect of heterogeneity. The result shows that the uncertainty of the soil parameters has the most significant effect on the global safety factor of the soldier-piled excavation or on the pullout resistance safety factor of the nails for case of soil nail wall.

The first aim of this study was to investigate the failure mechanism of pile-soil system by using the FEM software program (Plaxis 3D). Furthermore, the failure mechanism related to the various ratio of the distance to the diameter of piles (S/D) was also discussed. For the soil arching effect, Liang and Yamin (2010) used the load transfer factor (η) to quantify the effectiveness of the soil arching effect. However, η may also be affected significantly by different judgment methods (Lin *et al.* 2019). Since the mentioned methods are not directly quantified the soil arching effect on the safety factor (FoS), it is difficult to be adopted in practical engineering. Although 3D numerical analysis has been frequently used to evaluate slope stability, this complicated procedure is not widely accepted in practical engineering. By contrast, 2D and 3D slope stability charts are commonly adopted in practical engineering because they can be used to determine slope stability in an easy and rapid manner. Some slope stability charts are currently available for slopes without drilled shafts (Michalowski 2002, 2010, Deng *et al.* 2019, Sahoo *et al.* 2020). Therefore, the second aim of this study was to quantize the soil arching effect on the safety factor (FoS) for colluvium slopes with drilled shafts. For practicality, the geology and engineering conditions in Taiwan were adopted in the analysis. Finally, field cases were investigated to validate the suitability of the proposed stability charts.

2. Previous studies

According to the purposes of this study, the reviewed studies were divided into four categories, namely studies on colluvium in Taiwan, the strength reduction method (SRM), the soil arching effect, and failure surface determination. The aforementioned categories of studies are briefly reviewed in the following text.

Table 1 Parameters related to colluvium in Taiwan

No.	c'(kPa)	ϕ'(°)	γ, γ_{sat} (kN/m^3)	Location	Ref.
1	18.8	29.6	19.3, -	Shiding Dist., New Taipei City	Jeng and Sue (2016)
2	5	26	19, 21	Fanlu Township, Chiayi County	Lin *et al.* (2015)
3	7.4	30.0	20.2, -	Heping Dist., Taichung City	Shou *et al.* (2009)
4	6.10	27.30	19.5, 20.1	Wenshan Dist., Taipei City	Yang *et al.* (2017)

2.1 Colluvium in Taiwan

Colluvial soils are distributed throughout Taiwan (e.g., Shalunzai and Shiding in northern Taiwan, Lishan, Tsaoling, and Central Cross-Island Highway in central Taiwan, and Woo-Wan-Chai (Chiayi) and Jiasian (Kaohsiung) in southern Taiwan) because of its special geological and geographical environment. Therefore, slope-related disasters usually occur after typhoons and heavy rainfall in Taiwan (Shou *et al.* 2009, Jeng and Su 2016, Lee *et al.* 2013, Yang *et al.* 2017). Shou *et al.* (2009) combined limit equilibrium analysis and Monte Carlo analysis with a geographic information system to evaluate the soil stability of the Lishan area. Their results revealed that the slopes of the aforementioned area are stable under dry conditions but vary considerably under fully saturated conditions, which indicates that control and monitoring of the groundwater level are crucial tasks. On the basis of 15-year records of typhoon rainfall-induced slope failures along the Alishan Highway (covering the Woo-Wan-Chai area), Lee *et al.* (2013) indicated that rainfall is the direct cause of slope failure in the mountainous areas of Taiwan. Therefore, they adopted rainfall data, including the maximum hourly rainfall and effective cumulative rainfall, to develop an innovative empirical model for a slope management system. The failure of colluvial slopes is one of the main slope disasters in Taiwan. Thus, the stability problem of colluvial slopes warrants further study. In this study, the colluvium parameters and most commonly encountered slope conditions in Taiwan were collated (Table 1). Additionally, the range of the colluvium parameters was determined and used in the numerical analysis.

2.2 SRM

The SRM is a technique for calculating the FoS in the FEM. Zienkiewicz (1975) stated that the FEM uses the SRM step by step when the analysis equation cannot satisfy the convergent value in the balanced equation. In this case, the reduction factor is defined as the FoS. In addition, SRM is widely used for stability evaluation in engineering projects, including slope stability (Likitlersuang *et al*. 2018,

Ye *et al.*2020, etc.), surface stability for tunneling, and foundation (Jalili and Moosavi 2019). The evaluation of failure by using the SRM involves using the nodal displacement method (Donald and Giam 1988) and nonconvergence method of the numerical solution (Griffiths and Lane 1999). In this study, the nodal displacement method is adopted to evaluate the FoS. When the SRM is adopted to evaluate the FoS, the dilatancy angle (ψ') is a nonnegligible parameter. Tschuchnigg *et al.* (2015) assessed the effect of ψ' on the FoS stability by using a 2D numerical analysis model. They highlighted that high ψ' values and high slope angles under the nonassociated rule can easily yield instability. Lin *et al.* (2020) indicated that the dilatancy angle had different effects on the convergence of 3D and 2D slope models. The effect of ψ' on FoS convergence is less sensitive for lower soil strength parameters (c' and ϕ') than for higher soil strength parameters. Colluvium has low ψ' because of its loose structure, therefore, the effect of ψ' was negligible (ψ'=0°) in this study.

2.3 Soil arching effect and failure surface determination

The soil arching effect considerably affects the stability of slopes with drilled shafts. The concept of the soil arching effect was initially introduced by Terzaghi in 1943. Many researchers have conducted studies on enhancing the stability of unstable slopes by using drilled shafts or piles (Ito and Matsui 1975, Poulos 1995, Liang and Zeng 2002, Ramanandan and Dodagoudar, 2020, Neeraj and Thiyyakkandi 2020). In addition, the physical model test is a useful and efficient way to analyze landslide evolution and observe the interaction mechanisms between the piles and the sliding mass. (Zhang *et al.* 2018, Hu *et al.* 2019, Zhong *et al.* 2020). Zhang *et al.* (2018) monitored and analyzed, the Majiagou landslide in China, the deformation characteristics of the landslide-stabilizing pile system for three years. Their study showed piles could effectively provide local resistance and partially slowed down the sliding mass behind the piles. Hu *et al.* (2019) showed the differing deformation characteristics of rigid and flexible piles, and pointed out the rigid pile is more suitable for landslide control based on its deformation characteristics.

With regard to the influence of the soil arching effect on slope stability, Wang and Yen (1974) explored the influence of the soil arching effect for piles on a stiff and plastic infinite slope. Their study concluded that the strength parameters and the distances among the piles are important factors influencing the soil arching effect. In addition, Chen and Martin (2002) used the finite-difference method and loading-displacement curves for piles to interpret how stress is transferred from the soil to the piles. Liang and Zeng (2002) proposed an innovative design method in accordance with the soil arching effect and provided a quantitative definition of the load transfer factor (η) for the soil arching effect. The load transfer factor (η) is the ratio of horizontal force on the vertical surfaces between the piles on the lower side of the slope to that on the upper side, as displayed in Fig. 1. The corresponding equations are Eqs. (1) and (2).

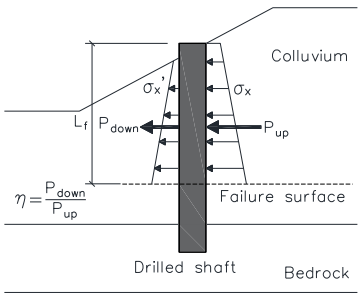

Fig. 1 Illustration of the load transfer factor (η)

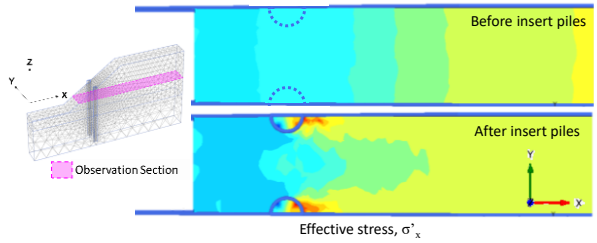

Fig. 2 Illustration of the horizontal stress (σ'_x) distribution with/without drilled shafts

$$0 \le \eta = \frac{P_{down}}{P_{up}} \le 1 \quad (1)$$

where P_{up} is the horizontal force on the vertical surface between the pile and the soil on the upper side of the slope and P_{down} is the horizontal force on the vertical surface between the pile and the soil on the lower side of the slope.

$$P_{up} = \int_0^{L_f} \int_0^n \sigma_x d_y d_z \qquad P_{down} = \int_0^{L_f} \int_0^n \sigma'_x d_y d_z \quad (2)$$

where n is the thickness of the longitudinal direction of the model (i.e., the center-to-center distance between two adjacent drilled shafts), L_f is the distance between the top of the drilled shafts and the failure surface, σ_x is the horizontal stress of the drilled shafts on the upper side of the slope, and σ'_x is the horizontal stress of the drilled shafts on the lower side of the slope.

Based on the adopted baseline model from Liang and Zeng (2002), Lin *et al.* (2013, 2019) conducted Plaxis 3D program to observe the change of σ'_x due to soil arching effect. The result shows the distribution of horizontal stress (σ'_x) is significantly different before and after the piles are inserted as shown in Fig. 2. In theory, η should be smaller than 1 and larger than 0. When η is equal to 1, the soil arching effect does not occur on the slopes. By contrast, when η is equal to 0, the drilled shafts behave as a retaining wall and shield off all soil stress from the upper slope area. According to Eq. (2), the value of η depends on the depth of the failure surface (L_f). However, it may also be affected significantly by different judgment methods (Lin *et al.* 2019). The FoS can be obtained directly using the SRM in FEM software to avoid the uncertainty of L_f. Therefore, in this study, the FoS was used instead of η to quantify the soil arching effect on slopes with drilled shafts.

Currently, numerous FEM software programs are available for evaluating failure surface parameters, such as

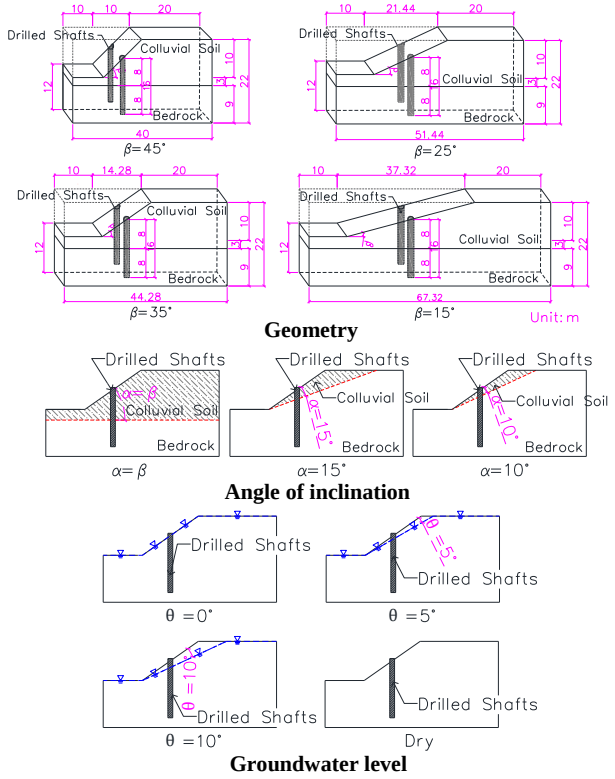

Fig. 3 Standard slope model used in this study

stress, strain, and displacement. This study observed the development of the failure surface according to the shear strain method. (Matsui and San 1992, Wei and Cheng 2009, Tschuchnigg *et al.* 2015)

3. Problem definition and numerical model

The aims of this study were to investigate the arching effects and failure mechanism of pile-soil system in colluvium slopes in Taiwan reinforced by the drilled shafts. A serial of numerical simulation using software program (Plaxis 3D) with the built-in strength reduction technique (SRM) was conducted. Fig. 3 showed the investigated slope models in this study. Three main materials were included in the model, the colluvium soil, the embed rock layer, and concrete piles. Based on Table 1, the range of the colluvium parameters (c' and ϕ') was determined and used in the numerical analysis. The bedrock layer is used to stabilize the bottom of the pile. The investigated range of parameters and model material characteristics are presented in Table 2. Overall, the developed models are based on four slope angles (β=15°, 25°, 35° and 45°), three tilts (α=β, 10° and 15°), four groundwater table levels (θ=0°, 5°, 10° and dry), and three S/D ratio (2, 3 and 4). In addition, a one-row pile placed in the middle of a slope was considered mainly in this study. The reasons for considering the mentioned variable (α, θ and S/D ratio) were briefly explained as follows:

• Rock inclination angle (α): According to the selected ranges of c' and ϕ', the failure mechanism was found to be shallow. When the rock inclination angle (α) was equal to the slope angle (β), it meant that the embed rock layer was horizontal and deep. Thus, the depth of the failure surface is not significantly influenced by the depth of the rock. Consequently, rock inclination angles (α) of 10° and 15° were considered to explore the influence of rock angle on rock formation, as displayed in Fig. 3. The deeper failure controlled by specific weak layer with very low ϕ' value was not considered in this study.

• Groundwater table levels (θ): Rainfall considerably influences slope stability in Taiwan. In fact, the groundwater table is a curve, and the FoS would be decreased when the failure surfaces cross the groundwater elevation. Therefore, the groundwater was simplified into a dip plane (θ=0°, 5°, 10°, and dry) through the failure zone to consider the effects of rainfall on slope stability. The consideration should be reasonable because the water table above the shallow failure surface is changed. On the other hand, the effects of earthquakes were not considered in this study but will be considered in future studies.

• S/D ratio: The preliminary study of various S/D ratio (S/D=2-5) was conducted to check the safety of pile using P-M curve based on the Taiwanese Design Code (Design Specifications for Concrete Structures, 2019). The result showed the pile could not bear the bending stress due to lateral force when the S/D≥5. Practically, using S/D≥5 for drilled shafts in Taiwan is also not common. Additionally, Ng *et al.* (2001) also pointed that the stress transfer mechanism between piles was very small when S/D>5. Overall, the S/D ratio=2, 3, 4 were considered, and pile material was reasonable to assume linearly elastic in this study.

• Number and position of piles: The remedy of multiple rows is rarely used to stabilize slopes in Taiwan which would be because of shallow failure surfaces. A one-row pile placed in the middle of a slope was considered in this study. In the case of piled slopes, the position of pile is a critical factor. Previous studies have indicated that the most effective location of drilled shafts is around the middle of the slope (Lee *et al.* 1995, Cai and Ugai 2000, Wei and Chen 2009, Liang and Yamin 2010, Li *et al.* 2012, Boulfoul *et al.* 2020). However, the study by Ausilio *et al.* (2001) showed the pile installation around the toe of the slope is the effective location. In the authors' opinion, the main reason is the failure surface getting deeper due to the lower ϕ' value was adopted by Ausilio *et al.* (2001). In fact, the assumption of ϕ'=10° would not be reasonable (Holtz *et al.* 2010). Although it is uncommon in Taiwan to use multiple rows or one-row piles not placed in the middle of the slope, the proposed methods still can be extended to cover the above-mentioned cases. They are presented in Section 4.3.3.

In general, 2D assessment is used for slope design and analysis (Yang *et al.* 2017, Qi *et al.* 2019, Hou *et al.* 2019), and the contribution of piles to slope stability is converted using the equivalence method. Thus, the 3D soil arching effect cannot be reflected. The soil arching effect can be illustrated using a simple 3D model with two piles. In this study, a simple 3D slope model was adopted to evaluate the contribution of the soil arching effect to slope stability. Any complex 3D slope can be simplified into several

Table 2 Parameters for the colluvium slope considering in this study

Category	Parameter	Value of the parameter
Properties of soil	ϕ'	20°-40°
	c'	0-15 kPa
	E_s*	9576 kPa
	γ, γ_{sat}	19.53, 20.1 kN/m^3
	v*	0.3
	ψ'	0°
	material model*	Mohr-Coulomb
	material property*	drained
Properties of rock*	E_r	2.4×10^7 kPa
	γ_r	26 kN/m^3
	v_r	0.2
	material model	linearly elastic
	material property	Non-Porous
Properties of pile*	diameter of piles (D)	1.0 m
	E_p	2×10^7 kPa
	γ_p	23.5 kN/m^3
	v_p	0.2
	material model	linearly elastic
	material property	Non-Porous
Geometry of the slope and arrangement of piles	slope angle (β)	15° 、25° 、35° 、45°
	angle of inclination (α)	10° 、15° 、β
	groundwater level (θ)	0° 、5° 、15° 、Dry
	ratio of the distance to the diameter of piles (S/D)	2 、3 、4
	location of piles	on the middle of slope
Property of interface**	soil-pile	R_{inter}=0.5

*Liang and Yamin (2010) ** Lin *et al*. (2019)

representative sections, and each section must be examined in practice. Although the aforementioned model is simple, it can satisfactorily represent most field conditions that may be encountered.

Fig. 4 displays a 3D view and boundary conditions of the drilled shaft/slope model used in the finite element simulations in this study. The right and left sides depicted in both views are allowed to move freely in the y and z directions but not in the x direction. In the bottom plane of the model, all movements are restrained (i.e., u, v, and w=0). A 3D FE mesh was generated automatically by the Plaxis 3D program (five mesh options, namely very coarse, coarse, medium, fine, and very fine), and tetrahedral elements with 10 nodes were used (the default option in Plaxis 3D). In this research, a preliminary study was conducted on five mesh density values for slopes without piles. When the very fine mesh option was adopted, the obtained safety factors were close to those obtained by Michalowski (2002). In addition, the FEM mesh was well refined at and near the region where the drilled shaft was located to enable close examination of the stress and displacement in that region. In summary, the model without piles is actually the longitudinal extension (y direction) of the 2D model, and there is no 3D boundary effect. When the piles are placed on both sides of the model, the arching

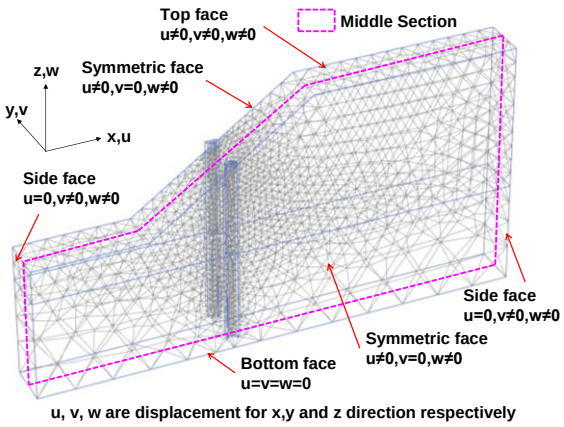

Fig. 4 Illustration of the boundary condition and meshes in the standard slope model (β=45° and S/D=4)

effect is generated between the piles, which is the main consideration in this study. In Plaxis 3D finite element code, the R_{inter} is used to consider the effect on interfaces between two materials. According to Plaxis Manual (2016), the R_{inter} could be assumed the order of 2/3 in the absence of detailed information. According to some studies, the R_{inter} is used form 0.5-0.9 (Dao 2011, Kim and Jeong 2009, Bryan and Brian 2014, Ampera and Aydogmus 2005, Potyondy 1961), and 0.5 is adopted in this study based on conservation.

It should be noted that the drilled shafts considered in this paper are not subjected to the vertical and lateral force from the structure (e.g., buildings or bridges). Additionally, there are no reinforcement facilities to enhance the piles, such as anchors or retaining walls.

4. Results and discussion

4.1 Numerical result

In this study, the drilled shafts are not subjected to a horizontal load at the head, or there are no reinforcement facilities to enhance the piles such as anchors or retaining walls. The obtained numerical results were validated and compiled and found to be suitable for presentation of using chart assessments. The stability charts are the direct method to reflect the contribution of soil arching effect and to provide a more convenient way to evaluate FoS for practical engineers. Taylor (1937) proposed the concept of a stability number. The analysis outcomes were used to develop a chart based on the stability number, which can be used for the efficient evaluation of slope stability. Numerous iterations are required when using the stability numbers of Taylor to obtain the FoS. Therefore, Bell (1966) changed the stability number to N* (see Eq. (3)) to obtain answers as quickly as possible.

$$N^* = \frac{c'_d}{\gamma H \tan\phi'_d} = \frac{c'/FoS}{\gamma H\left(\tan\phi'/FoS\right)} = \frac{c'}{\gamma H \tan\phi'} \quad (3)$$

where c' is the cohesion of the soil, γ is the unit weight of the soil, and H is the height of the slope.

In this study, the format of presented design charts is

Table 3 Comparisons of safety factors for the virtual slope with/without pile reinforcement under different β value

	β=15°					β=25°					β=35°					β=45°				
α	(a)	S/D=2		S/D=4		(a)	S/D=2		S/D=4		(a)	S/D=2		S/D=4		(a)	S/D=2		S/D=4	
		(b)	(c)	(b)	(c)		(b)	(c)	(b)	(c)		(b)	(c)	(b)	(c)		(b)	(c)	(b)	(c)
β	2.60*	3.12	20.0%	2.98	14.6%	1.75*	2.21	26.3%	2.05	17.1%	1.35*	1.77	31.1%	1.63	20.7%	1.07*	1.49	39.3%	1.36	27.1%
15°	2.72	3.15	15.8%	3.03	11.4%	1.85	2.21	19.5%	2.10	13.5%	1.43	1.77	23.8%	1.64	14.7%	1.14	1.49	30.7%	1.37	20.2%
10°	2.86	3.17	10.8%	3.07	7.3%	2.05	2.21	7.8%	2.15	4.9%	1.59	1.80	13.2%	1.66	4.4%	1.31	1.50	14.5%	1.41	7.6%

(a): Slope without pile reinforcement (b): Slope with pile reinforcement (c): $\Delta FoS = \frac{[(b)-(a)]}{(a)} \times 100\%$

*FoS obtained from Michalowski's (2002, 2010) stability charts

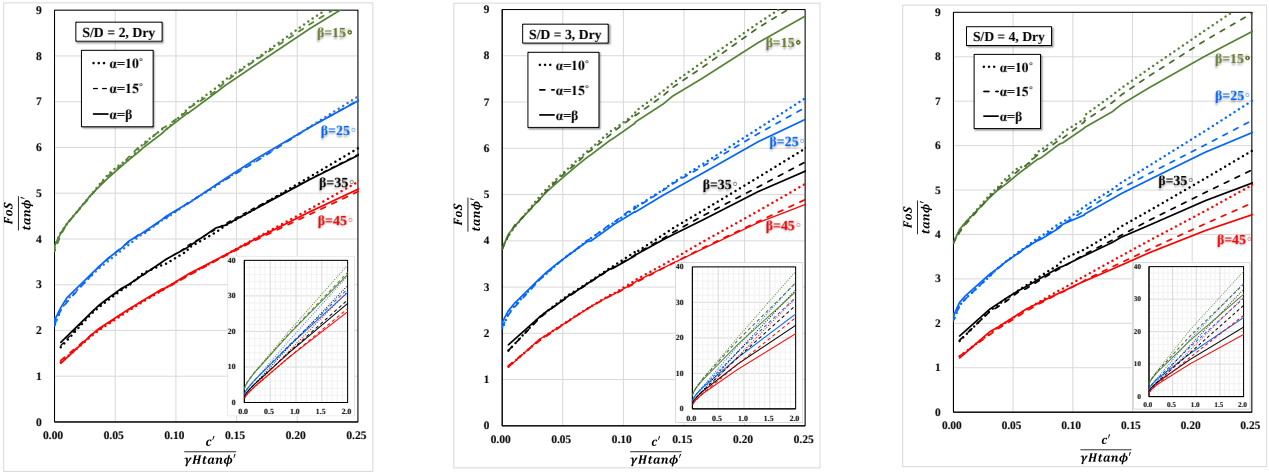

Fig. 5 Stability chart for the results obtained under various S/D ratios (water table=dry)

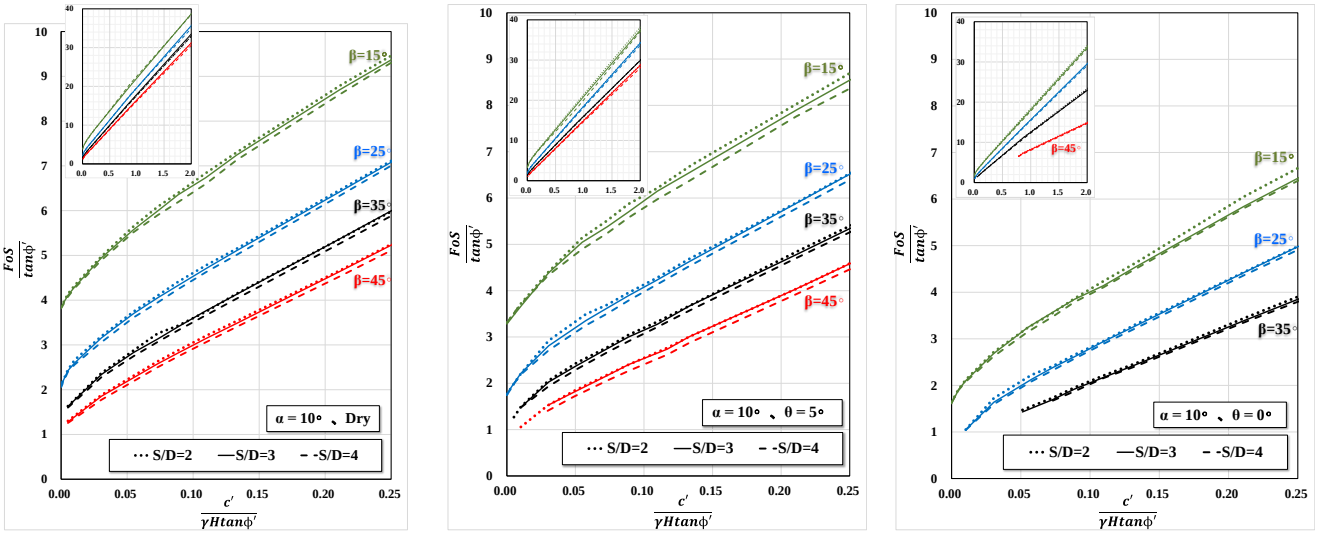

(a) α=10°

Fig. 6 Stability chart for the results obtained under various α and θ values

similar to those proposed by Bell (1966). Additionally, the stability number (N*) of the proposed charts is not limited to the colluvium soil but extended for a range of soil parameters. Fig. 5 shows the results obtained under various S/D ratios without groundwater table. It revealed that the FoS increases with increases in c' and ϕ'. Moreover, the β and S/D values are inversely proportional to slope stability. Thus, when the β and S/D, and values increase, the slope stability decreases.

A virtual slope with height=10 m and β=45° was adopted in this study to investigate the contribution of drilled shafts to slope stability. The angle of inclination and the groundwater table were not considered in this case (α=β, dry condition). The soil parameters were γ=20 kN/m^3, c'=10 kPa, and ϕ'=25°. For a slope without drilled shafts, the FoS was obtained as 1.07 from Michalowski's (2002, 2010) stability charts. When drilled shafts are adopted, the FoS is obtained with the proposed stability charts through the following three steps:

Step 1: Calculate the dimensionless parameters

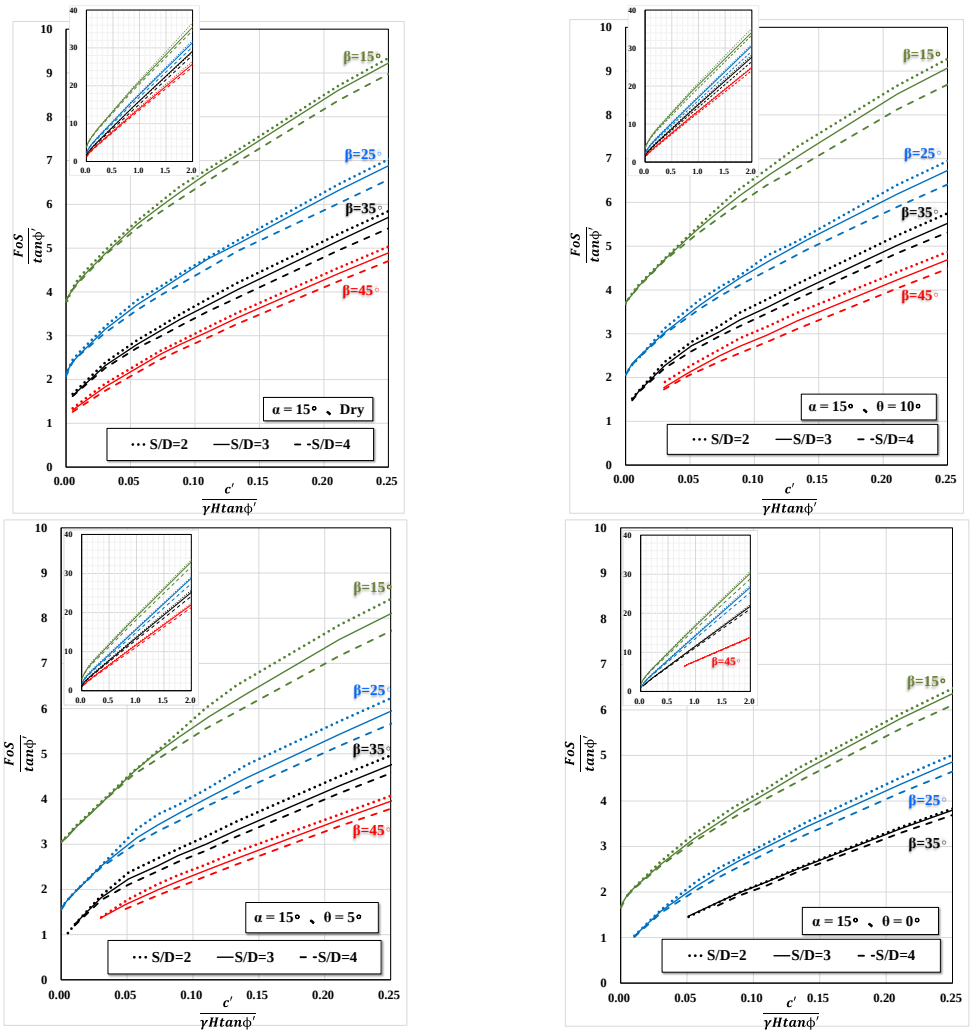

(b) α=15°

Fig. 6 Continued

($\frac{c'}{\gamma H \tan\phi'}$) according to the slope geometry and parameters.

Step 2: Obtain $\left(\frac{FoS}{\tan\phi'}\right)$ from the proposed stability charts for β and the S/D ratio.

Step 3: Calculate the FoS.

On the basis of the aforementioned calculation steps, FoS values of 1.49 and 1.36 were obtained for S/D values of 2 and 4, respectively, when α=β (Fig. 5). The aforementioned FoSs are respectively 39.3% and 27.1% higher than the FoS obtained from Michalowski's (2002, 2010) stability charts (1.07). Obviously, the increased rate of the FoS is due to the contribution of the soil arching effect. In addition, for α=10°, the FoS values were 1.50 and 1.41 when the S/D ratio was 2 and 4, respectively. The aforementioned FoS values are respectively 14.5% and 7.6% higher than the FoS of the slope without pile reinforcement (1.31). It was worth noting that the FoS difference (FoS=1.50-1.41) decreases when comparing to α=β. The reason was related to the failure surface mechanism and will be discussed in section 4.2.

Table 3 shows the contribution of soil arching effect to FoS based on the mentioned virtual slope with different β values. Overall, when α=β, the FoS rates (ΔFoS) were greatly increased due to the soil arching effect. When the α=10°, the FoS has increased substantially because of the confined failure surfaces, discussed in section 4.2. Moreover, when α=β, the ΔFoS increases with β increase, which shows the soil arching effect does improve the stability of the relatively steep slopes.

Fig. 6 shows the results of considering the four groundwater table levels (θ), including dry condition. The overall trend was similar to the dry scenario, with the main difference being the decrease in FoS due to increasing groundwater level. Additionally, the steep slopes (β=45°) were failed in the numerical initial state because of high groundwater level (θ=0°) when $\frac{c'}{\gamma H \tan\phi'} \leq 0.8$ was considered. As displayed in Figs. 5 and 6, when $\frac{c'}{\gamma H \tan\phi'}$ is relatively small (there is no exact value, but generally $\frac{c'}{\gamma H \tan\phi'} \leq 0.05$), the $\frac{FoS}{\tan\phi'}$ exhibits a minor discrepancy which can be ignored for different S/D and α. The main reason is that the failure surface on the slope has a shallow depth which could be affected by the mesh density and arrangement.

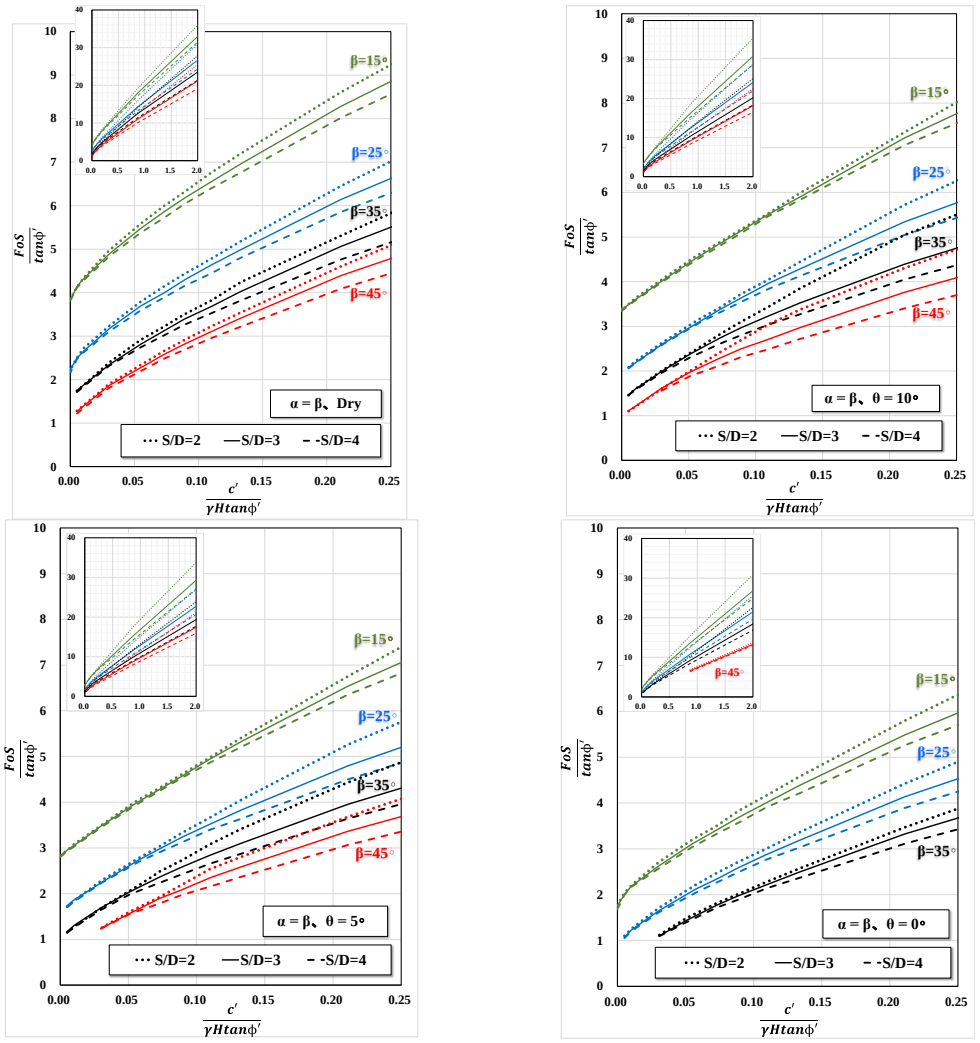

(c) $\alpha=\beta$

Fig. 6 Continued

4.2 Development of the failure surface

The slope using drilled shafts (passive piles) was the main consideration in this study. Unlike passive piles, the active piles subjected to a horizontal load at the head, the local failure zone in front of the pile is first occurred (Ng *et al.* 2001). In this study, the incremental shear strain ($\Delta\gamma_s$) method was adopted to investigate the failure mechanism with different S/D ratios.

The results are displayed in Figs. 7-10. Some findings obtained from the results are listed as follows:

• All of the results indicate that the depth of the failure surface decreases when β increases. After the placement of drilled shafts, the failure surface is divided into two areas. The failure surface on the upper part of the hillside exhibits greater variation than does that on the lower part of the hillside ($\Delta\gamma_s$ is larger for the upper part) because of gravity, as displayed in Fig. 7.

• Fig. 8 displays the condition of the failure surface for different groundwater table levels. The development of the failure surface is similar for the dry and full water conditions (θ=0°) except when β=35°. The failure surface on the lower part of the hillside changes considerably when the groundwater table changes from θ=0° to θ=10°,

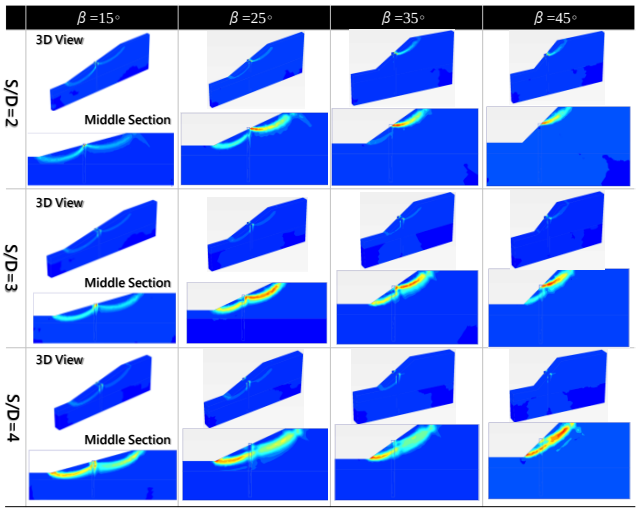

Fig. 7 Comparison of the failure surfaces obtained under different S/D and β values (c'=10 kN/m^2, ϕ'=25°, $\alpha=\beta$, and water table=dry)

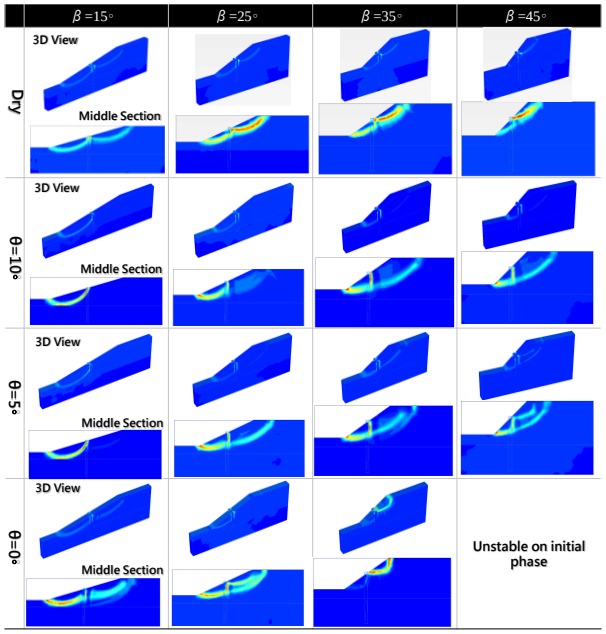

Fig. 8 Comparison of the failure surfaces obtained under different θ and β values (c'=10 kN/m^2, ϕ'=25°, S/D =3, and α=β)

primarily because the soil at the lower part of the slope becomes saturated.

• Fig. 9 displays the condition of the failure surface on α=β for different S/D values. When the S/D value is small (S/D=2), the development of the failure surface is suppressed by the soil arching effect. The main failure surfaces are located above the piles on the upper part of the hillside for all cases. When the S/D ratio increases, the soil arching effect decreases gradually. Therefore, the failure surface expands from the upper to the lower part of the slopes, and the depth of the failure surface increases. This phenomenon is consistent with that described by Wei and Cheng (2009).

• Comparison of the failure surfaces obtained under different S/D, α and β values is shown in Fig. 10. Overall, as α changes from β to 10°, it is clear that the failure surfaces begin to be confined by the rock layer. For example, Fig. 10(c) with β=45°, when S/D=4, the soil arching effect is greatly diminished and the failure surface could be regarded as slope without piles. The failure surface developed from the upper to the lower part of the slopes when α=β. As α changed to 10°, the failure surface was obviously restrained and could not pass to the lower part of the slope. At the same time, the FoS increases significantly when α changes from β to 10°. An example can be seen in Table 3, the FoS without pile reinforcement increases from 1.07 to 1.31 due to the confined failure surface.

• As mentioned virtual slope in the 4.1 section, when the S/D ratio was equal to 2, the FoS values for α=β and 10° only differed by 0.7% (FoS=1.49, 1.50). The primary reason is that the failure surfaces are restrained and located in the area above the pile locations, as shown in Fig. 10(a). The failure surfaces are shallow and almost unaffected by the α value. Thus, the FoS does not exhibit a substantial change. By contrast, when the S/D ratio increased to 4, the FoS

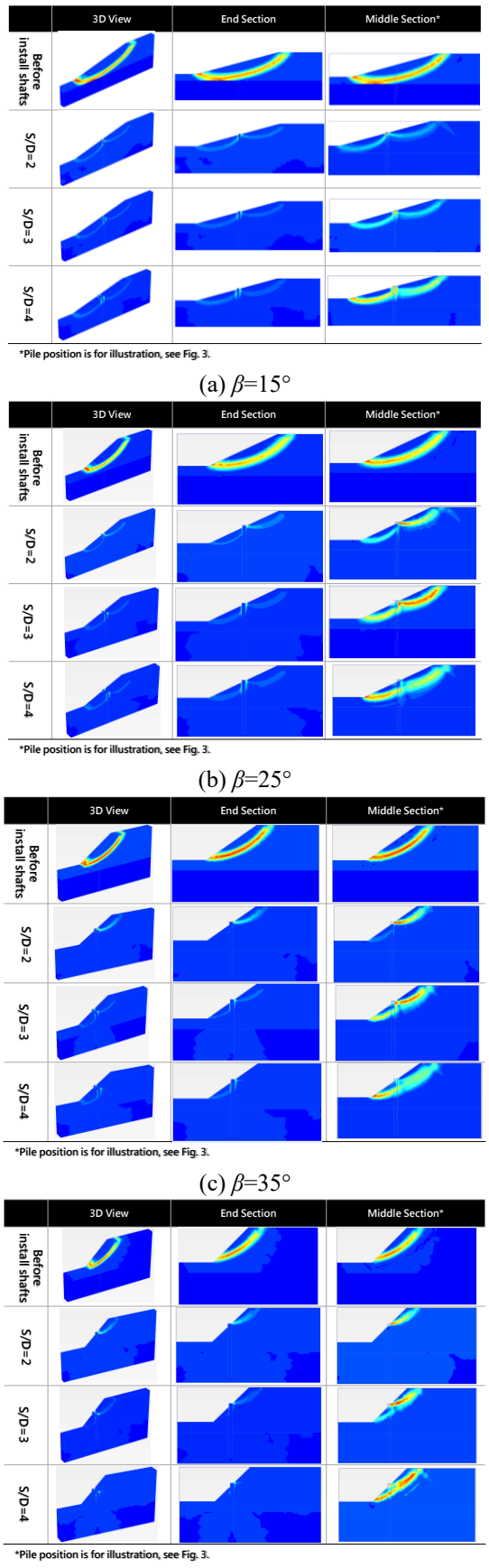

(a) β=15°

(b) β=25°

(c) β=35°

(d) β=45°

Fig. 9 Comparison of the failure surfaces obtained under different S/D ratios (c'=10 kN/m^2, ϕ'=25°, α=β, and water table=dry

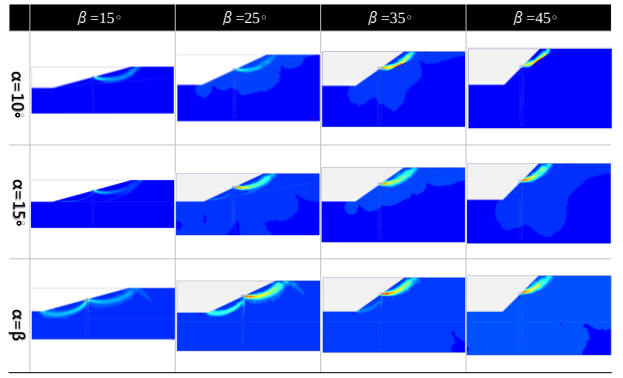

(a) S/D=2

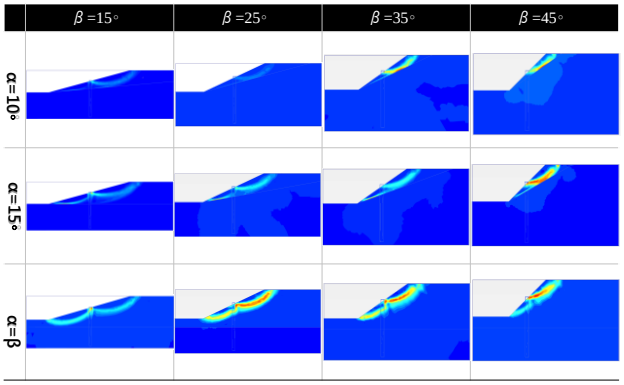

(b) S/D=3

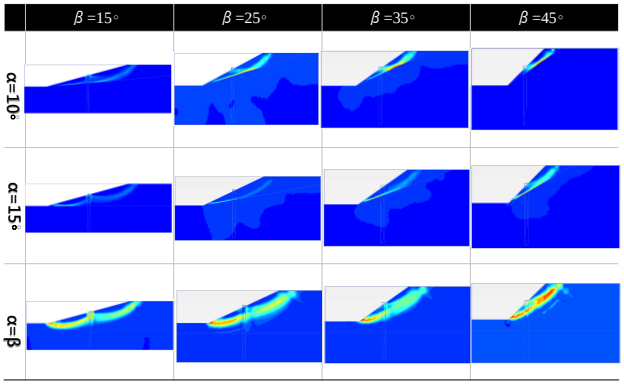

(c) S/D=4

Fig. 10 Comparison of the failure surfaces obtained under different α and β values (c'=10 kN/m2, ϕ'=25°, and water table=dry)

values for $\alpha=\beta$ and 10° differed by 3.7% (FoS=1.36, 1.41). Figs. 10(a)-(c) show the soil arching effect between piles diminishes gradually when the S/D ratio changes from 2 to 4. When S/D=4 and $\alpha=\beta$, the sliding surface expands and passed through the middle space of the piles because of the decreasing soil arching effect. When α=10°, the failure surfaces are still confined and located in the area above the pile locations for S/D=4, compared with those for S/D=2. It is the probable reason that the FoSs did not change substantially by increasing the S/D value.

4.3 Case studies and verification example

The colluvial slope remedy of applying drilled shafts in the Woo-Wan-Chai area in Taiwan was the first case

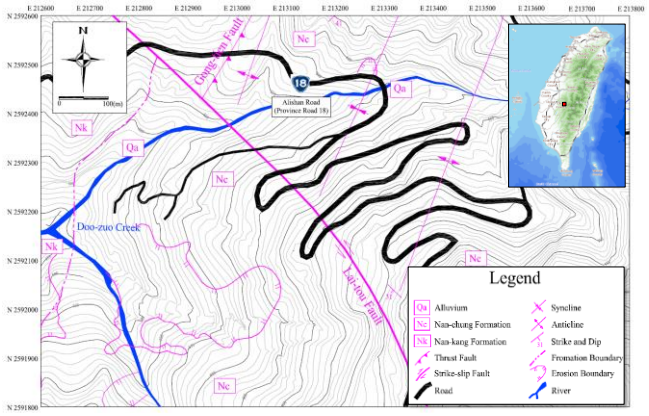

Fig. 11 Regional geology of Woo-Wan-Chai

analyzed for validating the proposed charts. Furthermore, a field case published in the literature was studied (Li and Liang 2014) to verify the accuracy and rationality of the proposed design charts.

4.3.1 Woo-Wan-Chai case in Alishan in Taiwan

Province Road 18 (Alishan Highway) is a critical road that leads to Alishan. Because of the weak geologic structure and complex combinations of various soil types along the road, numerous slope collapses occur during the rainy season, periods of heavy rainfall, and typhoons. These slope collapses cause road closures and endanger the safety of passengers. The collapsing area in this case, which was situated 30 m east of Chiayi city in Gongtian Village, Fanlu Town, Chiayi County, was approximately 50 ha. The road is called Woo-Wan-Chai because of the steep topography between Province Road 8 28K+900 and 31K+500, which makes the shape of the road similar to five Zs (Fig. 11).

The collapsing area of Woo-Wan-Chai was the middle part of the slope on the western side of the Alishan mountains. The elevation is higher in the eastern part of this hillside than in the western part, and the slope angle is approximately 23°. In addition, the elevation of the aforementioned slope decreases from 772 to 580 m over a horizontal distance of 470 m. The slope is an east-west edge that sinks into Doo-zuo Creek. Headward erosion is vigorous in the southern tributary upstream of Doo-zuo Creek. This erosion contributed to the formation of numerous valleys, gullies, and small collapses in the southwestern part of Woo-Wan-Chai, leading to slope instability in this area (Fig. 11).

The collapsing area in Woo-Wan-Chai belonged to a landslide area in the western foothills of the Western mountains, whose basement rocks are the rocks of the Miocene Nan-Chung Formation. The basement rocks primarily include light-gray sandstone, sandstone, interbedded shale, and dark-gray shale.

Moreover, the basement rocks are covered with yellowish brown weathered rock mass and colluvium. The strike of the strata is in the north-south or northeast-southwest direction near the investigated area. The strata tilt toward the east or west by 10° to 60°. In addition, one anticline and one syncline exist along the northeast-southwest direction of the aforementioned area. The Lai-tou

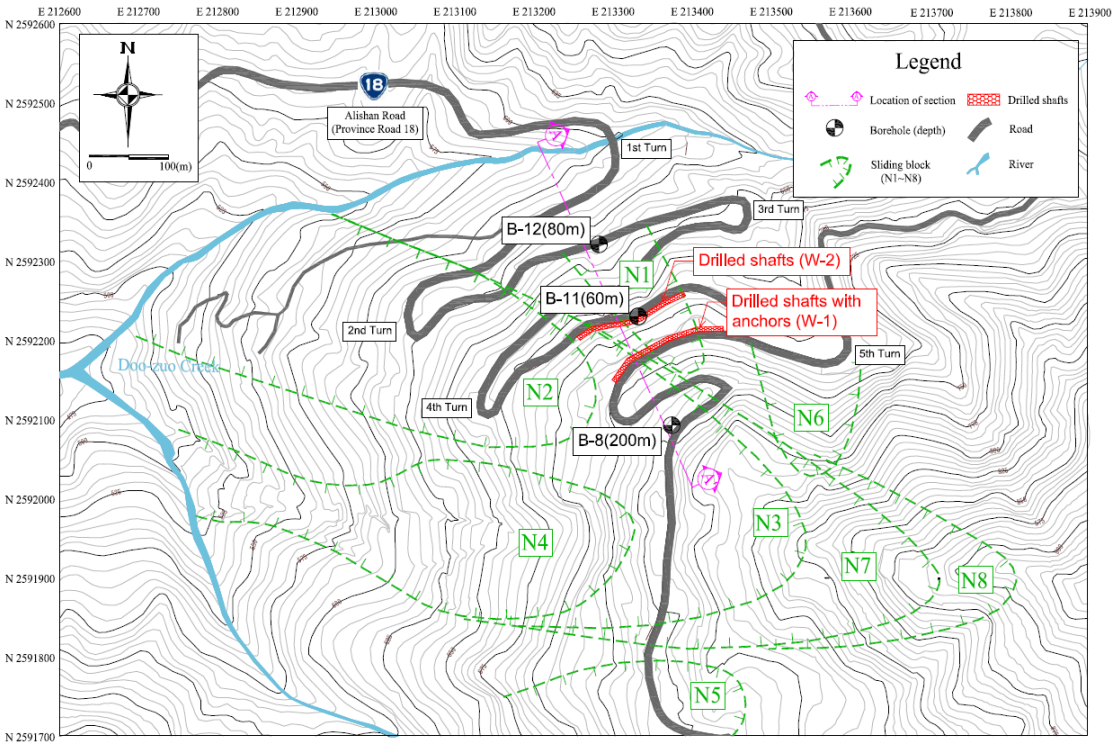

(a) Locations of sliding blocks, boreholes, and drilled shafts

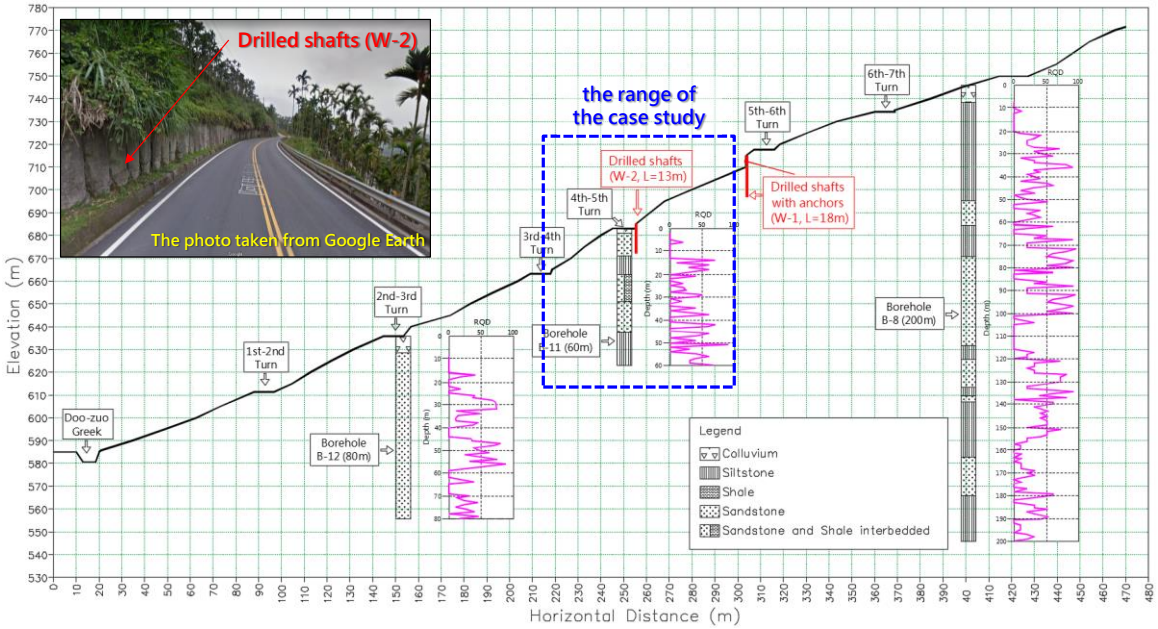

(b) A-A-section

Fig. 12 Locations of boreholes and the cross-section of Woo-Wan-Chai (base map: Land Engineering Consultants Co., Ltd., 2006)

Fault cuts through the edge of the southwestern part of this area along the northwest-southeast direction. Numerous geological structures cross the collapsing zone in Woo-Wan-Chai, resulting in broken strata. Therefore, this area is prone to landslides (Fig. 11). The report of Land Engineering Consultants Co., Ltd. (2006) indicates that the sliding blocks (N1-N8) of the collapsing area in Woo-Wan-Chai has eight potential sliding directions oriented toward Doo-zuo Creek. The N4 sliding block collapsed in 2003. The adjacent N3 sliding block is the most active sliding block and has first priority for remediation. Because the N2 block is a part of the N3 block and has an obvious sliding trend, N2 has second priority for remediation. Furthermore, N1 is not on the list for remediation because of its lack of an obvious sliding tendency (Fig. 12(a)).

Because the N2 and N3 sliding blocks continued to move after the collapse of N4, the DGH decided to advance construction of the fourth curve in 2007. Two retaining

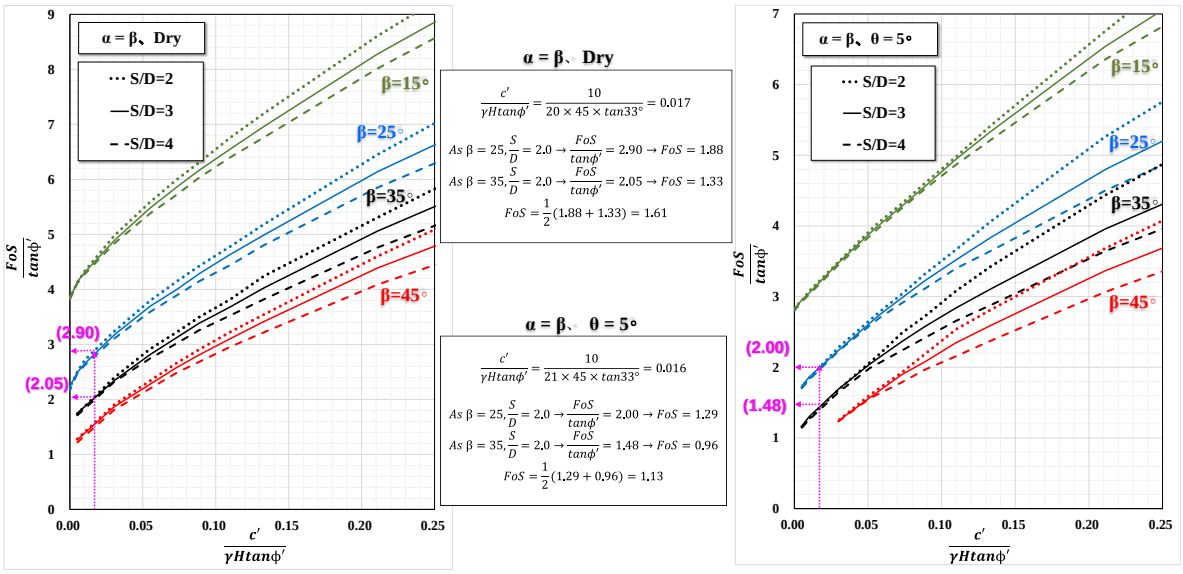

Fig. 13 Search result for the slope with retaining shear piles in Woo-Wan-Chai

piles, namely W-1 (height=18 m) and W-2 (height=13 m), were adopted to stabilize the slope and maintain road service (Fig. 12(b)). These two retaining piles had a diameter of 1 m and were spaced 1-m apart (i.e., S/D=1). Anchors were added on top of the W-1 pile to increase overall stability except that of the retaining pile. The W-2 pile is only the retaining piles. This study primarily focused on retaining piles. Hence, the slope for W-2 was used to verify the proposed charts. The geometry and soil parameters of the slope for W-2 were mainly determined with reference to the studies of Lin *et al.* (2015) and Land Engineering Consultants Co., Ltd. (2006). The height of the slope (H) was 45 m (elevation=662-707 m), and the slope angle (β) was approximately 30°. The study area had two geological layers. The upper layer comprised gray colluvial soil with a thickness of 1.5-8.2 m. The thickness of this soil decreased from the upper to lower part of the slope. The unsaturated unit weight (γ) and saturated unit weight (γ_{sat}) of the slope were 20 and 21 kN/m^3 respectively. The soil cohesion (c') was 10 kPa, and the soil internal friction angle (ϕ') was 33°. The lower layer comprised gray shale. The retaining piles had a diameter of 1 m, lined the intersections of cross-sections, and were located in the middle of the slope. Because some drainage wells were set up in the study area to reduce water pressure, the groundwater level (θ=5°) could be used to represent the rainfall conditions.

The value of β was 30°, and this result could not be obtained using only one chart. Consequently, the average outcome is considered. The calculation procedure illustrated in Fig. 13 is briefly described as follows:

• The dimensionless parameters were calculated according to the geometry and parameters of the hillside.

Normal condition (without rainfall or earthquakes):

$$\frac{c'}{\gamma H \tan\phi'} = \frac{10}{20\times45\times\tan 33°} = 0.017$$

Rainfall condition (without earthquakes):

$$\frac{c'}{\gamma H \tan\phi'} = \frac{10}{21\times45\times\tan 33°} = 0.016$$

• Because the dimensionless parameters were small, the influence of the S/D became negligible. Consequently, β was the only consideration during the search. The $(\frac{FoS}{\tan\phi'})$ value was obtained from the slope stability charts for β=25° and 35°.

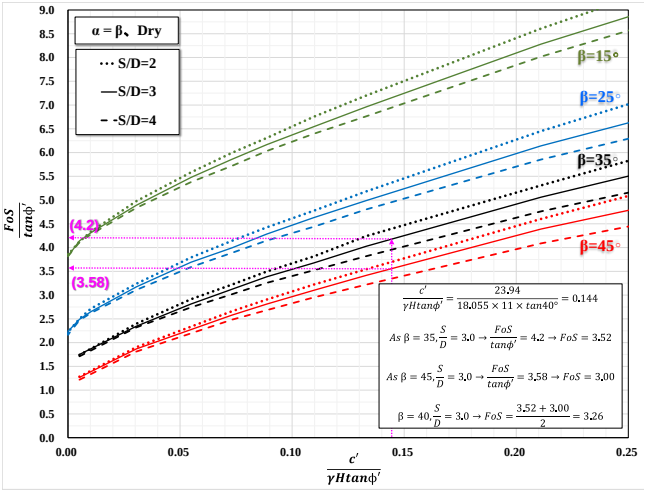

Fig. 14 Search result for the FoS for the case of Li and Liang (2014)

Normal condition:

$\frac{FoS}{\tan\phi'}$=2.90 → FoS=1.88 (for β=25°)

$\frac{FoS}{\tan\phi'}$=2.05 → FoS=1.33 (for β=35°)

Rainfall condition:

$\frac{FoS}{\tan\phi'}$=2.00 → FoS=1.29 (for β=25°)

$\frac{FoS}{\tan\phi'}$=1.48 → FoS=0.96 (for β=35°)

• The FoS for the slope with drilled shafts was calculated.

Normal condition:

FoS=(1.88+1.33)/2=1.61

Rainfall condition:

FoS=(1.29+0.96)/2=1.13

According to the slope stability charts, the FoS values for normal and rainfall conditions were 1.61 and 1.13,

respectively, which satisfy the FoS values in the design code for slopes in Taiwan (1.5 and 1.1 for normal and rainfall conditions, respectively). According to the survey report of Land Engineering Consultants Co., Ltd. (2006), the Woo-Wan-Chai landslide was a large-scale landslide, which is beyond the scope of this study. In this study, only the safety of the local slope with drilled shafts was examined. The LEM was also employed in the Geostudio program (slope/W) to obtain the FoS for normal conditions. The FoS values obtained with the Bishop method and general LEM were 1.522 and 1.516, respectively, which are very close to the recommended value of 1.5 in the design code for slopes in Taiwan.

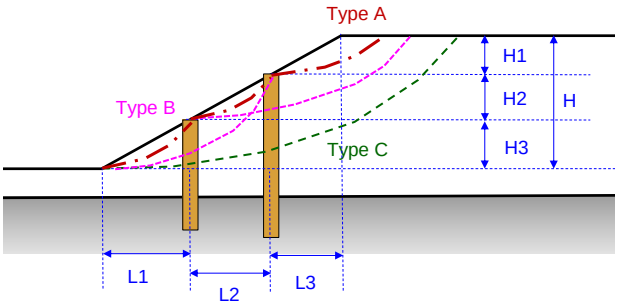

Fig. 15 Illustration of different failure surfaces with multiple drilled shafts

4.3.2 Landslide case of Li and Liang

The slope with drilled shafts studied by Li and Liang (2014) (No. 17 case) is verified. This slope had a height of 11 m and a β value of 40°. The γ, c', and ϕ' values of the aforementioned slope were 18.055 kN/m^3, 23.94 kPa, and 40°, respectively. Moreover, the S/D was assumed to be 3 in the middle of the slope (ζ=L_x/L=0.5). The FoS was 3.1 after pile installation.

To determine the FoS for the aforementioned slope, the results were averaged because β was 40° and could not be determined from a single chart. The procedure used for the calculations displayed in Fig. 14 is described as follows:

• The dimensionless parameters were calculated according to the geometry and parameters of the slope.

$$\frac{c'}{\gamma H \tan\phi'} = \frac{23.94}{18.055\times11\times\tan 40^\circ} = 0.144$$

• The value of $\frac{FoS}{\tan\phi'}$ was obtained from the stability charts for β=35° and 45° separately when the S/D ratio was 3.

$$\frac{FoS}{\tan\phi'} = 4.20 \rightarrow \text{FoS} = 3.52 \text{ (for } \beta = 35^\circ)$$

$$\frac{FoS}{\tan\phi'} = 3.58 \rightarrow \text{FoS} = 3.00 \text{ (for } \beta = 45^\circ)$$

• The FoS for the slope with drilled shafts was calculated as follows:

$$\text{FoS} = (3.52+3.00)/2 = 3.26$$

According to the proposed stability charts, the FoS of the aforementioned slope was 3.26. The FoS obtained by Li and Liang (2014) was 3.1. The difference between the two results is 0.16 (approximately 4.9%). Thus, the proposed charts are reasonable and feasible.

4.3.3 Cases of multiple-row or single-row piles not in the middle of the slope

A slope with a two-row pile was used to illustrate the application of the obtained stability charts in a multirow case (Fig. 15). In general, failure surfaces can be divided into three types: Type A, Type B, and Type C.

Type A failure surfaces are restricted by piles. Type B and Type C failure surfaces pass through a single-row and two-row pile, respectively. In the case of Type A failure surfaces, the slope can be divided into three parts without drilled shafts. The FoS of each part can be obtained using the method of Michalowski (2002) or the charts presented in this paper. The difference in the FoS values between the aforementioned two approaches is small and acceptable (0.018-0.084), as displayed in Fig. 16. For Type A and Type B failure surfaces, the proposed design charts can be used directly to obtain the FoS. However, for Type C failure surfaces, the obtained charts are not applicable.

If the drilled shafts are not located at the center of the slope, then the proposed design charts can be applied using the extended slope method, as depicted in Fig. 17. This method involves extending the slope length (L is adjusted to 2L1) and height (H is adjusted to 2H1), with the piles at the

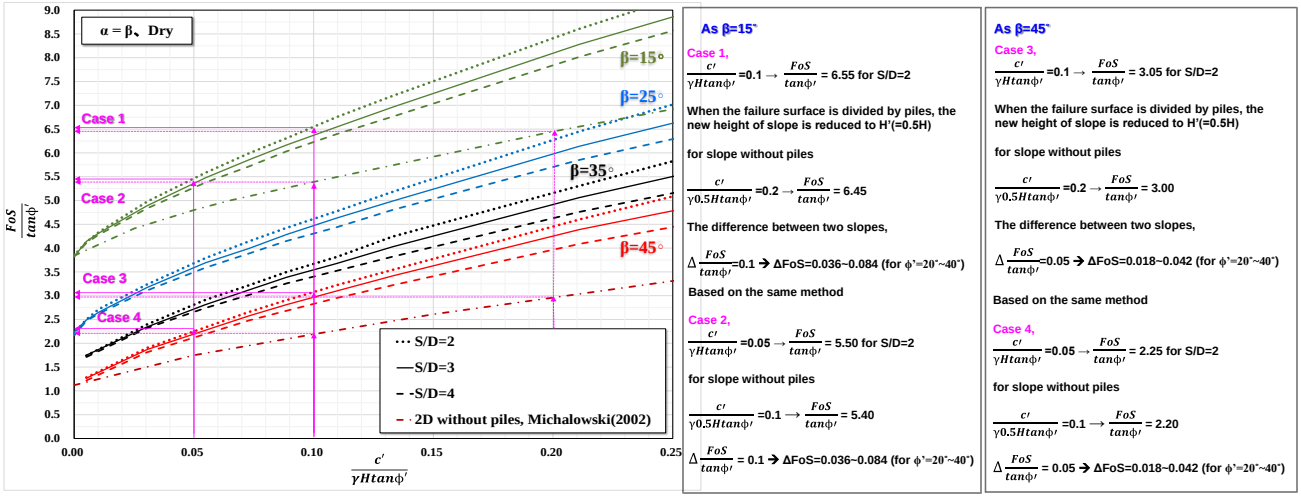

Fig. 16 Comparison of the FoS values obtained with and without drilled shafts for failure surface A

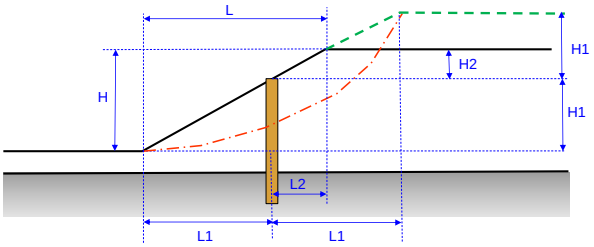

Fig. 17 Method used when the pile was not placed in the middle of the slope

center of the slope. The FoS can then be obtained for the new height (2H1) and length (2L1). The obtained FoS is a conservative value.

Consider the case in Section 4.3.3 as an example. All of the geometric and soil parameters are the same, however, the pile location is moved to the upside of the slope (i.e., $\zeta=L_x/L$=0.8, H1=0.8H=8.8 m). According to the proposed method, the modified slope height is 17.6 m (2H1) and the dimensionless parameter is 0.09. The FoS is 2.60 for the slope with drilled shafts (where the FoS is 2.85 and 2.35 when β=35° and 45°, respectively). The obtained result indicates that the FoS decreases from 3.26 to 2.60 if the pile location is moved to the upper side of the slope, which verifies that the most effective location for drilled shafts is near the middle of the slope (Lee *et al.* 1995, Cai and Ugai 2000, Wei and Chen 2009, Yamin and Liang 2010).

5. Conclusions

In this study, Plaxis 3D was employed to investigate the failure mechanism of pile-soil system and quantize the soil arching effect for colluvium slopes reinforced by drilled shafts. Moreover, it was found that the results can be presented using chart solutions. Some presented cases were also investigated to validate the suitability of the proposed charts, including Woo-Wan-Chai case in Alishan. According to the results obtained in this study, the following conclusions and suggestions are presented:

• In this study, the development of failure surfaces on slopes with drilled shafts was evaluated through examination of incremental shear strain. The obtained outcome is reasonable. The failure mechanism is influenced by the S/D ratio, which also reflects the contribution of the soil arching effect to slope stability. When $\alpha=\beta$ and the S/D ratio increases by a factor of 4, the failure surface of the slope is not significantly influenced by the piles.

• This study shows that using drilled shafts is an effective remedy for colluvium slope stabilization. Overall, the soil arching effect is more significant on $\alpha=\beta$ and is more efficient to the stability of the steep slopes.

• The slope stability charts proposed in this paper were developed according to the numerical results, and the contribution of soil arching effect on FoSs of the slopes with drilled shafts was quantified. The overall trend of the charts is consistent with those presented in relevant studies on slopes without drilled shafts. In addition, the results obtained for two adopted cases (including Woo-Wan-Chai case in Taiwan) indicate that the proposed stability charts are reliable. The proposed stability charts are not only suitable for colluvial slopes in Taiwan but also for general slopes with drilled shafts. As long as the slope conditions (e.g., the soil parameters, slope geometry, geological conditions, and pile shape, etc.) are in accordance with the assumptions in this study, the proposed charts could be used for preliminary FoS assessment.

• Although the remedy of multiple rows is rarely used to stabilize colluvial slopes in Taiwan, this study also provides a conservative approach to evaluate FoS for slopes with multiple rows. In addition, if the single-row piles are not in the middle of the slope, the proposed charts can be applied using the extended slope method suggested in this study.

Acknowledgments

The authors thank Land Engineering Consultants Co., Ltd. for providing information and investigation reports on the Woo-Wan-Chai case. The financial support provided by the Ministry of Science and Technology, Taiwan, is also gratefully acknowledged.

References

Ashour, M. and Ardalan, H. (2012), "Analysis of pile stabilized slopes based on soil-pile interaction", *Comput. Geotech.*, **39**, 85-97. https://doi.org/10.1016/j.compgeo.2011.09.001.

Ausilio, E., Conte, E. and Dente, G. (2001), "Stability analysis of slopes reinforced with piles", *Comput. Geotech.*, **28**, 591-611. https://doi.org/10.1016/S0266-352X(01)00013-1.

Bell, J.M. (1966), "Dimensionless parameters for homogeneous earth slopes", *J. Soil Mech. Found. Div.*, **92**(5), 51-65.

Boulfoul, K., Hammoud, F. and Abbeche, K. (2020), "Numerical study on the optimal position of a pile for stabilization purpose of a slope", *Geomech. Eng.*, **21**(5), 401-411. http://doi.org/10.12989/gae.2020.21.5.401.

Brinkgreve, R.B.J., Swolfs, W.M. and Engin, E. (2016), PLAXIS 3D 2016-User Manual, Delft, The Netherlands.

Bryan, A.M. and Brian, B.S. (2014), "Pile group settlement estimation: Suitability of nonlinear interaction factors", *Int. J. Geomech.*, **13**(3). https://doi.org/10.1061/(ASCE)GM.1943-5622.0000395.

Cai, F. and Ugai, K. (2000), "Numerical analysis of the stability of a slope reinforced with piles", *Soil. Found.*, **40**(1), 73-84. https://doi.org/10.3208/sandf.40.73.

Chen, C.Y. and Martin, G.R. (2002), "Soil-structure interaction for landslide stabilizing piles", *Comput. Geotech.*, **29**, 363-386. https://doi.org/10.1016/S0266-352X(01)00035-0.

Cho, G.C. (2016), "Geotechnical engineering for sustainable development", *Proceedings of the 2016 World Congress on Advances in Civil, Environmental and Materials Research (ACEM16)*, Jeju, Korea, August.

Chow, Y.K. (1996), "Analysis of piles used for slope stabilization", *Int. J. Numer. Anal. Meth. Geomech.*, **20**(9), 635-646. https://doi.org/10.1002/(SICI)1096-9853(199609)20:9<635::AID-NAG839>3.0.CO,2-X.

Dao, T.P.T. (2011), "Validation of PLAXIS embedded piles for lateral loading", Master Thesis, Delft University of Technology, The Netherlands.

Deng, D.P., Li, L. and Zhao, L.H. (2019), "Stability analysis of slopes under groundwater seepage and application of charts for optimization of drainage design", *Geomech. Eng.*, **17**(2), 181-

194. https://doi.org/10.12989/gae.2019.17.2.181.
Design Code (2019), Design Specifications for Concrete Structures, Construction and Planning Agency Ministry of the Interior, Taiwan.
Donald, I.B. and Giam, S.K. (1988), "Application of the nodal displacement method to slope stability analysis", *Proceedings of the 5th Australia-New Zealand Conference on Geomechanics. Sydney*, Australia.
Gholampour, A. and Johari, A. (2019), "Reliability-based analysis of braced excavation in unsaturated soils considering conditional spatial variability", *Comput. Geotech.*, **115**, 103163. https://doi.org/10.1016/j.compgeo.2019.103163.
Griffiths, D.V. and Lane, P.A. (1999), "Slope stability by finite elements", *Geotechnique*, **49**(3), 387-403. https://doi.org/10.1680/geot.1999.49.3.387.
Hassiotis, S., Chameau, J.L. and Gunaratne, M. (1997), "Design method for stabilization of slopes with piles", *J. Geotech. Geoenviron. Eng.*, **123**(4), 314-323. https://doi.org/10.1061/(ASCE)1090-0241(1997)123:4(314).
Holtz, R.D., Kovacs, W.D. and Sheahan, T.C. (2010), *An Introduction to Geotechnical Engineering*, 2nd Edition, Upper Saddle River, NJ, Pearson Prentice-Hall.
Hou, C., Zhang, T., Sun, Z., Dias, D., and Li, J. (2019), "Discretization technique for stability analysis of complex slopes", *Geomech. Eng.*, **17**(3), 227-236. http://doi.org/10.12989/gae.2019.17.3.227.
Hu, X., Zhou, C., Xu, C, Liu, D., Wu, S. and Li, L. (2019), "Model tests of the response of landslide-stabilizing piles to piles with different stiffness", *Landslid.*, **16**, 2187-2200. https://doi.org/10.1007/s10346-019-01233-4.
Ito, T. and Matsui, T. (1975), "Methods to estimate lateral force acting on stabilizing piles", *Soil. Found.*, **15**(4), 43-59. https://doi.org/10.3208/sandf1972.15.4_43.
Jalili, J. and Moosavi, M. (2019), "Evaluation of the truncated soldier pile behavior in an anchored deep excavation case study by the aid of 3d and 2d finite element analyses", *J. GeoEng.*, **14**(3), 191-202. http://doi.org/10.6310/jog.201909_14(3).7.
Jeng, C.J. and Su, D.Z. (2016), "Characteristics of ground motion and threshold values for colluvium slope displacement induced by heavy rainfall: a case study in northern Taiwan", *Nat. Hazard. Earth Syst Sci.*, **16**, 1309-1321. https://doi.org/10.5194/nhess-16-1309-2016.
Johari, A. and Kalantari, A.R. (2021), "System reliability analysis of soldier-piled excavation in unsaturated soil by combining random finite element and sequential compounding methods", *Bull. Eng. Geol. Environ.*, **80**, 2585-2507. https://doi.org/10.1007/s10064-020-02022-3.
Johari, A., Hajivand, A.K. and Binesh, S. (2020), "System reliability analysis of soil nail wall using random finite element method", *Bull. Eng. Geol. Environ.*, **79**, 2777-2798. https://doi.org/10.1007/s10064-020-01740-y.
Kim, Y.H. and Jeong, S.S. (2011), "Analysis of soil resistance on laterally loaded piles based on 3D soil-pile interaction", *Comput. Geotech.*, **38**, 248-257. https://doi.org/10.1016/j.compgeo.2010.12.001.
Land Engineering Consultants Co., Ltd. (2006), "Fieldwork report of Woo-wan-chai landslide area, 28km+900-31 km+500, Province Road 18", Report to Fifth District, Directorate General Highway, Taiwan. (in Chinese)
Lee, C.Y., Hull, T.S. and Poulos, H.G. (1995), "Simplified pile-slope stability analysis", *Comput. Geotech.*, **17**, 1-16. https://doi.org/10.1016/0266-352X(95)91300-S.
Lee, D.H, Lai, M.H., Wu, J.H., Chi, Y.Y., Ko, W.T. and Lee, B.L. (2013), "Slope management criteria for Alishan Highway based on database of heavy rainfall-induced slope failures", *Eng. Geol.*, **162**, 97-107. https://doi.org/10.1016/j.enggeo.2013.04.012.
Li, L. and Liang, R.Y. (2014), "Reliability-based design for slopes reinforced with a row of drilled shafts", *Int. J. Numer. Anal. Meth. Geomech.*, **38**, 202-220. https://doi.org/10.1002/nag.2220.
Li, X., Pei, X., Gutierrez, M. and He, S. (2012), "Optimal location of piles in slope stabilization by limit analysis", *Acta Geotechnica*, **7**, 253-259. https://doi.org/10.1007/s11440-012-0170-y.
Liang, R.Y. and Yamin, M. (2010), "Three-dimensional finite element study of arching behavior in slope/drilled shafts system", *Int. J. Numer. Anal. Meth. Geomech.*, **34**, 1157-1168. https://doi.org/10.1002/nag.851.
Liang, R.Y. and Zeng, S. (2002), "Numerical study of soil arching mechanism in drilled shafts for slope stabilization", *Soil. Found.*, **42**(2), 83-92. https://doi.org/10.3208/sandf.42.2_83.
Likitlersuang, S., Pholkainuwatra, P., Chompoorat, T., Keawsawasvong, S. (2018), "Numerical modelling of rail way embankment for high-speed train constructed on soft soil", *J. Geoeng.*, **13**(3), 149-159. http://doi.org/10.6310/jog.201809_13(3).6.
Lin, D.G., Chen, W.H. and Wang, S.H. (2015), "Three-dimensional numerical analyses of the mechanical behaviors of retaining shear piles stabilized slope", *J. Chin. Soil Water Conserv.*, **46**(4), 205-212. (in Chinese)
Lin, H.D., Li, A.J. and Wang, W.C. (2019), "Investigation of load transfer factor of slope with drilled shaft", *Proceedings, 16th Asian Regional Conference on Soil Mechanics and Geotechnical Engineering*, Taipei.
Lin, H.D., Tjuar, R. and Dang, H.P. (2013), "Analyses of drilled shaft effects on stabilizing the soil slope", *1st Taiwan-Kazakhstan Joint Workshop in Geotechnical Engineering*, Taipei, Taiwan.
Lin, H.D., Wang, W.C. and Li, A.J. (2020), "Investigation of dilatancy angle effects on slope stability using the 3D finite element method strength reduction technique", *Comput. Geotech.*, **118**, 103295. https://doi.org/10.1016/j.compgeo.2019.103295.
Michalowski, R.L. (2002), "Stability charts for uniform slopes", *J. Geotech. Geoenviron. Eng.*, **128**(4), 351-355. https://doi.org/10.1061/(ASCE)1090-0241(2002)128:4(351).
Michalowski, R.L. (2010), "Limit analysis and stability charts for 3D slope failures", *J. Geotech. Geoenviron. Eng.*, **136**(4), 583-593. https://doi.org/10.1061/(ASCE)GT.1943-5606.0000251.
Nakamura, H. (1984), "Design of rigid dowel piles for landslide control", *4th International Symposium on Landslides*, **2**, 149-154.
Neeraj, C.R., and Thiyyakkandi, S. (2020), "Estimation of lateral pile resistance incorporating soil arching in pile-stabilized slopes", *Geomech. Eng.*, **23**(5), 481-491. http://doi.org/10.12989/gae.2020.23.5.481.
Ng, C.W.W. and Zhang, L.M. (2001), "Three-dimensional analysis of performance of laterally loaded sleeved piles in sloping ground", *J. Geotech. Geoenviron. Eng.*, **127**(6), 499-509. https://doi.org/10.1061/(ASCE)1090-0241(2001)127:6(499).
Poulos, H.G. (1995), "Design of reinforcing piles to increase slope stability", *Can. Geotech. J.*, **32**, 808-818. https://doi.org/10.1139/t95-078.
Qi, S., Vanapalli, S.K., Yang, S.G., Zhou, J.W., and Lu, G.D. (2019), "Stability analysis of an unsaturated expansive soil slope subjected to rainfall infiltration", *Geomech. Eng.*, **19**(1), 1-9. http://doi.org/10.12989/gae.2019.19.1.001.
Ramanandan, S., and Dodagoudar, G.R. (2020), "Reliability analysis of slopes stabilized with piles using response surface method", *Geomech. Eng.*, **21**(6), 513-525. http://doi.org/10.12989/gae.2020.21.6.513.
Sahoo, P.P., Shukla, S.K. and Ganesh, R. (2020), "Taylor's slope stability chart for combined effects of horizontal and vertical seismic coefficients", *Geotechnique*, **70**(9), 835-838. https://doi.org/10.1680/jgeot.17.P.222.
Shou, K., Chen, Y. and Liu, H. (2009), "Hazard analysis of Li-

shan landslide in Taiwan", *Geomorphology*, **103**, 143-153. https://doi.org/10.1016/j.geomorph.2007.09.017.
Stewart, D.P. (1992), "Lateral loading of piled bridge abutments due to embankment construction", Ph.D. Dissertation, University of Western Australia.
Stewart, D.P., Jewell, R.J. and Randolph, M.F. (1994), "Design of piled bridge abutments on soft clay for loading from lateral soil movements", *Geotechnique*, **44**(2), 277-296. https://doi.org/10.1680/geot.1994.44.2.277.
Taylor, D.W. (1937), "Stability of earth slopes", *J. Boston Soc. Civil Eng.*, **24**(3), 197-246.
Tschuchnigg, F., Schweiger, H.F. and Sloan, S.W. (2015), "Slope stability analysis by means of finite element limit analysis and finite element strength reduction techniques. Part I: Numerical studies considering non-associated plasticity", *Comput. Geotech.*, **70**, 78-189. https://doi.org/10.1016/j.compgeo.2015.06.018.
Wang, D.L. and Yen, B.C. (1974), "Soil arching in slopes", *J. Geotech. Eng.*, **104**(4), 493-496. https://doi.org/10.1061/AJGEB6.0000005.
Wei, W.B. and Cheng, Y.M. (2009), "Strength reduction analysis for slope reinforced with one row of piles", *Comput. Geotech.*, **36**, 1176-1185. https://doi.org/10.1016/j.compgeo.2009.05.004.
Yang, K.H., Uzuoka, R., Thuo, J.N., Lin, G.L. and Nakia, Y.T. (2017), "Coupled hydro-mechanical analysis of two unstable unsaturated slopes subject to rainfall infiltration", *Eng. Geol.*, **216**, 13-30. https://doi.org/10.1016/j.enggeo.2016.11.006.
Ye, S.H., Zhao, Z.F. and Zhu, Y.P. (2020), "Dynamic response analysis of loess slope reinforced by frame anchors based on numerical simulation and shaking table test", *J. GeoEng.*, **15**(2), 89-101. http://doi.org/10.6310/jog.202006_15(2).3.
Zhang, Y., Hu, X., Tannant, D.D., Zhang, G. and Tan, F. (2018), "Field monitoring and deformation characteristics of a landslide with piles in the Three Gorges Reservoir area", *Landslid.*, **15**, 581-592. https://doi.org/10.1007/s10346-018-0945-9.
Zhong, Z., Yong, R., Tang, H., Li, C. and Du, S. (2020), "Experimental studies on the interaction mechanism of landslide stabilizing piles and sandwich-type bedrock", *Landslid.*, **18**, 1369-1386. https://doi.org/10.1007/s10346-020-01570-9.
Zienkiewicz, O.C., Humpheson, C. and Lewis, R.W. (1975), "Associated and non-associated visco-plasticity and plasticity in soil mechanics", *Geotechnique*, **25**(4), 671-689. https://doi.org/10.1680/geot.1975.25.4.671.

CC